CHEMISTRY OF MATERIALS
Cite This: Chem. Mater. 2019, 31, 8794−8800
Article
pubs.acs.org/cm

Kinetics Features Conducive to Cache-Type Nonvolatile Phase-Change Memory

Bin Chen,[†,‡] Yimin Chen,[§,∥] Keyuan Ding,[†,‡] Kunlong Li,[†] Fangying Jiao,[†] Lei Wang,[†] Xierong Zeng,[†] Junqiang Wang,[⊥] Xiang Shen,[∥] Wei Zhang,[#] Feng Rao,*[,†,∇] and Evan Ma[○]

[†]College of Materials Science and Engineering and [‡]Key Laboratory of Optoelectronic Devices and Systems of Ministry of Education and Guangdong Province, College of Optoelectronic Engineering, Shenzhen University, Shenzhen 518060, China

[§]Department of Microelectronic Science and Engineering, School of Physical Science and Technology and [∥]Laboratory of Infrared Material and Devices & Key Laboratory of Photoelectric Materials and Devices of Zhejiang Province, Advanced Technology Research Institute, Ningbo University, Ningbo 315211, China

[⊥]CAS Key Laboratory of Magnetic Materials and Devices & Zhejiang Province Key Laboratory of Magnetic Materials and Application Technology, Ningbo Institute of Materials Technology & Engineering, Chinese Academy of Sciences, Ningbo 315201, China

[#]Center for Advancing Materials Performance from the Nanoscale, State Key Laboratory for Mechanical Behavior of Materials, Xi'an Jiaotong University, Xi'an 710049, China

[∇]State Key Laboratory of Functional Materials for Informatics, Shanghai Institute of Micro-system and Information Technology, Chinese Academy of Sciences, Shanghai 200050, China

[○]Department of Materials Science and Engineering, Johns Hopkins University, Baltimore, Maryland 21218, United States

Supporting Information

ABSTRACT: Cache-type phase-change random-access memory is a remaining challenge on the path to universal memory. The recently designed $Sc_{0.2}Sb_2Te_3$ (SST) alloy is one of the most promising phase-change materials (PCMs) to overcome this challenge, as it allows subnanosecond crystallization speed to reach the crystalline ("1") state at elevated temperatures (e.g., 600 K) but years of reliable retention of the amorphous ("0") state for data storage at room temperature. This contrast in kinetics behavior, upon a relatively small temperature excursion, is more dramatic than that in other PCMs. From the temperature dependence of the crystallization kinetics uncovered via ultrafast differential scanning calorimetry, here, we report an apparent fragile-to-strong crossover in the SST supercooled liquid. We illustrate that two factors are at work simultaneously. First, Sc-stabilized precursors serve as heterogeneous sites to catalyze nucleation, reducing the stochasticity and thereby accelerating the nucleation rate. Second, the SST exhibits an enlarged kinetic contrast between elevated and ambient temperatures. Together they constitute a recipe for the design of PCMs that meets the needs of cache-type nonvolatile memory.

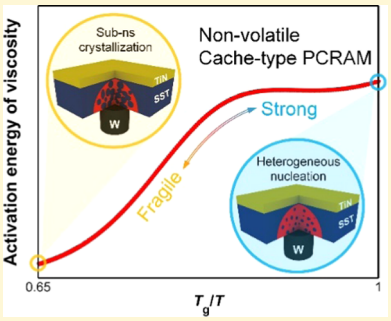

INTRODUCTION

Phase-change random-access memory (PCRAM), encoding digital information through reversible transformation between amorphous and crystalline states of chalcogenide phase-change materials (PCMs),[1−5] is the leading candidate among emerging nonvolatile memories for renovating current computing systems, where shuttling data among hierarchical memories, i.e., static random-access memory (SRAM), dynamic random-access memory (DRAM), and solid-state drive (SSD) flash memory, has long been of low efficiency.[6,7] Commercialized PCRAM products, employing the flagship PCM, i.e., $Ge_2Sb_2Te_5$ (GST), can operate on the order of tens of nanoseconds,[8,9] while reliably storing data for tens of years in the power-off states.[2,10] The fast and yet nonvolatile PCRAM can thereby serve as an encompassing bridge across the memory wall between volatile DRAM and nonvolatile SSD.[6,8] Recently released Intel's Optane DC chips already outperform SSD and begin to compete with DRAM.[11] The next challenge on the path to "universal memory" is the development of cache-type nonvolatile PCRAM with subnanosecond programming speed and, meanwhile, years of data retention to rival SRAM.[6,7]

One approach to address this challenge was recently shown by an innovative PCM alloy design.[12] This advance stemmed from the realization that the speed bottleneck of PCRAM devices lies in the relatively sluggish SET (crystallization) operation and not the RESET (amorphization) process.[13,14] In fact, the growth of crystals in supercooled liquid GST is already rather fast with the maximum velocity of several meters per second at ~600−700 K,[15] but the preceding nucleation of the

Received: July 1, 2019
Revised: October 10, 2019
Published: October 11, 2019

DOI: 10.1021/acs.chemmater.9b02598
Chem. Mater. 2019, 31, 8794−8800

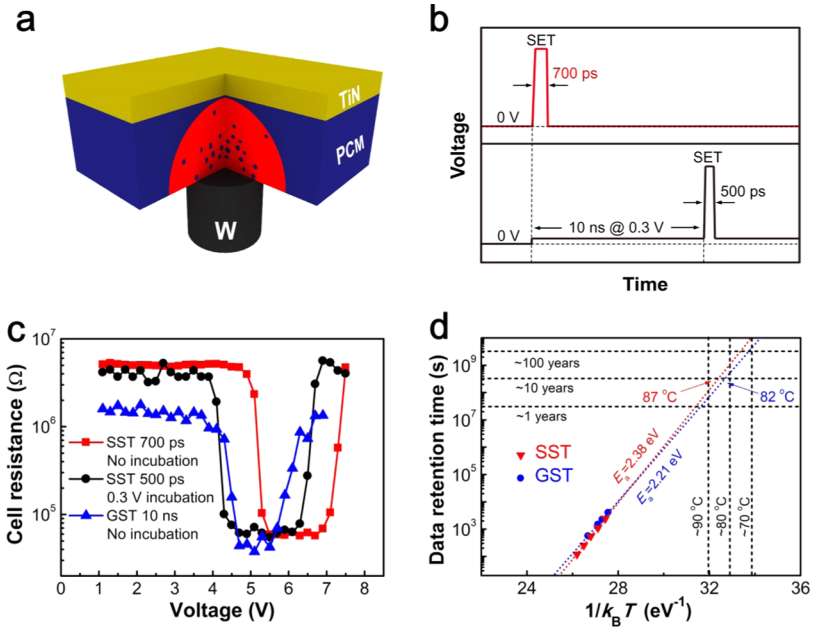

Figure 1. (a) Schematic of the SST- and GST-based T-shaped PCRAM devices with the same geometry, i.e., ∼150 nm-thick PCM layer, ∼20 nm-thick TiN top electrode, and ∼190 nm in diameter W bottom electrode. The mushroom-like area (red) represents the supercooled liquid phase with small nuclei/grains (blue) formed during crystallization. Upon SET operation, both materials show nucleation-dominated crystallization behaviors. (b) The electrical pulse waveform with and without the pretreatment/incubation (∼10 ns at 0.3 V) to SET the SST devices. (c) Resistance−voltage characteristics of SST devices with and without incubation action, as well as that for the GST device without incubation. (d) 10-Year data retention abilities for SST and GST devices. The data were fitted using the Arrhenius equation $t = A \exp(E_a/k_B T)$, where t is the time to failure when cell resistance of RESET state, at a certain isothermal heating temperature, falls to half of its initial magnitude, A is a proportionality constant, E_a is the activation energy, and k_B is the Boltzmann constant.

crystals is stochastic and time-consuming, which typically needs an incubation time of several hundreds of picoseconds to many nanoseconds.[16−19] Simply doping or adjusting the stoichiometry of GST and related materials usually enhances the metastability of the amorphous phase, but this inadvertently delays the crystallization of the latter.[20,21] The two goals are seemingly conflicting and a trade-off seems inevitable.[22]

Recently, we designed a $Sc_{0.2}Sb_2Te_3$ (SST) compound that enabled a 700 ps SET operation speed in a conventional PCRAM device, and yet its RESET state showed a good data retention ability,[12] evading the aforementioned trade-off between speed and retention. It was elucidated that the Sc addition provides a high density of precursors without appreciably reducing the atomic mobility at elevated temperatures (∼600−700 K), leading to an increased nucleation rate in the SET operation. In regard to the good thermal stability of amorphous SST, it was speculated that the Sc addition also effectively suffocates diffusion at low temperatures toward 300 K. In this work, we provide direct evidence of an enormous difference in the kinetics of SST, i.e., a diffusivity/viscosity contrast by many orders of magnitude, inside the supercooled liquid state over a fairly narrow temperature range. We suggest that besides the enhanced nucleation, the enlarged kinetic contrast for crystal growth serves as a second critical parameter for cache-type nonvolatile PCRAM.

RESULTS AND DISCUSSION

Pretreatment and Data Retention. As reported in ref 12, using a large mushroom-type device (Figure 1a), the SST compound we designed showed ultrafast nucleation, shortening the SET time into a subnanosecond regime. To further clarify the role of nucleation in SST devices, here we applied a 10 ns pretreatment pulse of 0.3 V to help incubate the nuclei, with a subsequent main pulse to complete the SET operation (Figure 1b). Such a priming action shortened the SET time in GST devices from ∼10 ns to 500 ps.[23,24] But for SST, such pretreatment only reduced the SET time to 500 ps (Figure 1c), merely shaving 200 ps off the 700 ps SET time of the SST device without pretreatment, in stark contrast with the case of GST devices.[23] We therefore conclude that (i) unlike the long incubation time needed for GST, in SST the incubation time for nucleation is intrinsically short (on the order of 200 ps) and (ii) the crystal growth in SST after nucleation appears to be as fast as that in GST.

The much-accelerated crystallization kinetics at elevated temperatures of SST over GST may implicate a weakened stability of the amorphous RESET state in the former at room temperature. However, this was shown not to be the case.[12] As reproduced in Figure 1d, the 10-year data retention ability of the RESET state for the SST device (∼87 °C) is even slightly better than that of the GST device (∼82 °C). The activation energy of crystallization (E_a) for the SST device (∼2.38 eV) estimated from Figure 1d is also a bit larger than that of the GST device (∼2.21 eV). These data suggest that crystallization is drastically suppressed in amorphous SST near room temperature, relative to that at elevated temperatures in the SET operation, despite the enhanced driving force for crystallization. To support this hypothesis, we performed ultrafast differential scanning calorimetry (DSC)[15,25] measurements on SST thin films to assess the crystallization kinetics as a function of temperature.

Crystal Growth Velocity. For PCMs, a simplified method was developed by Orava[15] and several other groups[26,27] to

DOI: 10.1021/acs.chemmater.9b02598
Chem. Mater. 2019, 31, 8794−8800

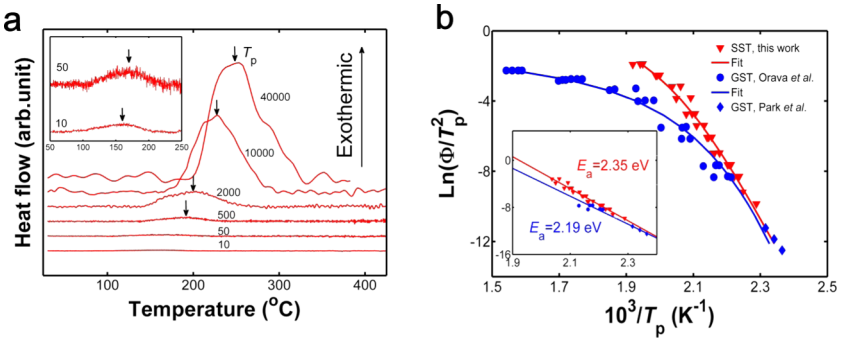

Figure 2. (a) Representative ultrafast DSC traces of SST thin films with Φ ranging from 10 to 40 000 K·s^{-1}. The inset zooms in the crystallization peak temperature (T_p) at low Φ. (b) The Kissinger plots show the ultrafast DSC data of SST and GST (by Orava et al.[15]) thin films, as well as several data points derived from conventional DSC for GST (by Park et al.[32]). The crystallization activation energy E_a for GST and SST is derived via linear fitting of respective data in the lower Φ range, as shown in the inset.

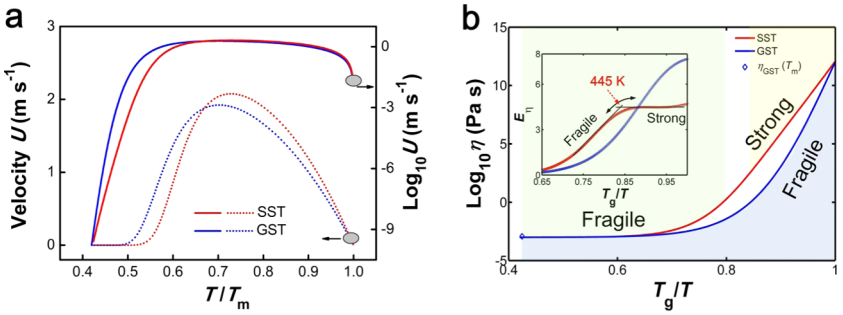

Figure 3. (a) Crystal growth velocities U of SST and GST supercooled liquids between T_g and T_m. (b) T_g-scaled temperature dependence of viscosity η, denoting an obvious fragile-to-strong (FTS) crossover of SST, which is not observed in GST. The simulated viscosity of GST at T_m in ref 18 is also depicted in (b), showing consistency with our fitting results. The activation energy of viscosity E_η for SST reaches a plateau when quenched toward T_g, while that of GST increases monotonically, as shown in the inset. An inflection temperature of ∼445 K is determined as the fragile-to-strong crossover point of SST.

analyze ultrafast DSC data to derive the crystal growth velocity. On continuous heating to crystallize a glass, with increasing temperature, the peak of the nucleation rate usually precedes the peak of the growth rate. An example was shown by ref 28 where the nucleation becomes progressively slower than the growth for temperatures greater than ∼450 K. One can then simplify the picture to assume that in a constant-heating-rate DSC scan, nucleation has been finished before the peak, which corresponds primarily to the main transformation of the volume by growth of a fixed population of nuclei.[15,29] The temperature dependence of the growth rate can then be obtained from Kissinger analysis of the shift of the peak position. The crystal growth velocities in PCM thin films derived in such ultrafast DSC experiments are known to match well with the values measured on real PCRAM devices.[30,31]

As done before in ultrafast DSC experiments performed on many PCMs,[15,25−27] we used heating rates (Φ) from 10 to 40 000 K·s^{-1} to crystallize the as-deposited amorphous SST films with a thickness of 300 nm. Several representative DSC traces, after background subtraction, are shown in Figure 2a, where the crystallization peak temperature (T_p, indicated by the arrows) shifts from ∼437 to ∼513 K upon increasing Φ from 10 to 40 000 K·s^{-1}. The shift of T_p allows for the investigation of crystallization kinetics at elevated temperatures. Note that the lowest 2−3 T_p values at each Φ were regarded as the most credible data because they correspond to the best thermal contact between stripped-off SST films and DSC chip sensors.[26,27] The crystallization data of SST via ultrafast DSC measurements are portrayed in the Kissinger plot (Figure 2b). GST data from ref 15 (ultrafast DSC) and ref 32 (conventional DSC) were also included for a direct comparison. SST obeys a linear relation across a wide Φ range in the Kissinger plot, complying with the Arrhenius behavior up to Φ > 10 000 K·s^{-1}, after which the Arrhenius behavior breaks down. Within the Arrhenius range, the fitted Kissinger plot gives a slope of E_a ∼ 2.35 eV (inset of Figure 2b), which is similar to the one (∼2.38 eV) from Figure 1d. In contrast, GST departs from the Arrhenius behavior (with E_a ∼ 2.19 eV) at a rather low heating rate (Φ ∼ 100 K·s^{-1}). The broader Arrhenius behavior of SST is analogous to those observed in AIST films[25] and GST nanoparticles.[26] In line with previous literature treatments, we have employed the same viscosity model (the generalized MYEGA model), combined with Johnson−Mehl−Avrami−Kolmogorov (JMAK) theory, to numerically simulate and fit the ultrafast DSC data of SST and GST supercooled liquids (see the Supporting Information for details).

Through fitting the Kissinger plots in Figure 2b, we obtained the temperature-dependent crystal growth velocity (U) for SST and GST supercooled liquids (see eq S1 and Discussions in the Supporting Information). In our JMAK modeling[15] here, nucleation is assumed to be time- and temperature-independent; the nucleation stage is finished at saturated sites before the DSC peaks. It is known that this simplification does not significantly alter the kinetics results derived as compared to the method adopting a more intricate nucleation model.[26] This scenario is in fact particularly appropriate for the heterogeneous crystallization case for SST, as will be discussed

DOI: 10.1021/acs.chemmater.9b02598
Chem. Mater. 2019, 31, 8794−8800

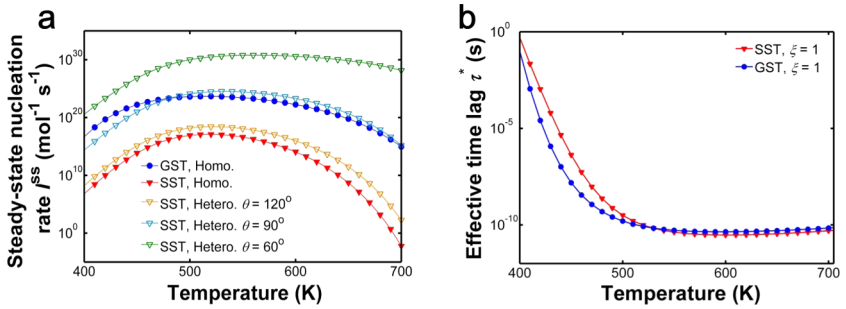

Figure 4. (a) Steady-state nucleation rate I^{ss} of GST (homogeneous, abbreviated as Homo.) and SST (Homo. and heterogeneous, abbreviated as Hetero., with the contact angle θ being 60, 90, and 120°). (b) The effective time lag (τ^*) of homogeneous nucleation for SST and GST supercooled liquids. In both the modeling, the Stokes−Einstein relation with decoupling parameter ξ = 1 was adopted.

later. The growth velocity results are shown in Figure 3a. Interestingly, the maximum growth velocity (U_{max}) (~2.07 m·s^{-1}) of SST, appearing at ~0.73 T_m (melting temperature, assumed to be ~890 K of Sb_2Te_3), is slightly higher than that of GST (U_{max} ~ 1.92 m·s^{-1} at ~0.70 T_m, with T_m being ~900 K). The U_{max} for GST agrees reasonably well with previous reports, in the range of ~0.5−3 m·s^{-1}.[15,26,30,31] Crystallization takes place in the supercooled liquid, above the glass-transition temperature (T_g) of ~371 and ~378 K for SST and GST, respectively, taken as usual to be the temperature where viscosity reaches 10^{12} Pa·s. Our T_g of GST is comparable with the previously reported ~383 K.[15] The temperature dependence of viscosity η (Figure 3b) is determined from the generalized-MYEGA model (see eq S3 and Discussions in the Supporting Information).

In between T_g and T_m, strong liquids such as silica follow Arrhenius behavior with a nearly constant activation energy for viscous flow, whereas fragile liquids, e.g., o-terphenyl,[33] exhibit a rather high activation energy near T_g but become markedly less viscous as the temperature increases. The Stokes−Einstein relation in the Arrhenius case ensures the atomic diffusivity D being inversely proportional to viscosity η, i.e., $U \propto D \propto \eta^{-1}$. When this relation breaks down, there will be decoupling between U and η, resulting in $U \propto \eta^{-\xi}$ with $\xi < 1$, i.e., an even faster crystal growth. Via fitting, the ξ for GST and SST can be estimated to be ~0.67 and ~0.65, respectively. Hence, as their η is almost equal at above ~570 K (i.e., T_g/T < ~0.65, as shown in Figure 3b), they have comparable U (the U of SST is ~1.1 times that of GST), as shown in Figure 3a. Note that in between T_g and $T_g/T \approx 0.65$, i.e., ~371−570 K, SST has a much larger η (<~100 folds) than GST (Figure 3b), corresponding to markedly slower U (<~120 times) than the latter in the T range from ~0.43 to ~0.65 T_m, i.e., ~380−580 K (Figure 3a). Clearly, the one-order-of-magnitude faster SET speed of the SST devices over the GST ones cannot be explained by the difference in U and therefore should not be attributed to crystal growth.

Fragile-to-Strong Crossover. The non-Arrhenius behavior of fragile liquids is characterized by fragility m, which is defined as the slope of the η at T_g, i.e., $m = d[\log_{10}\eta(T)]/d(T_g/T)|_{T=T_g}$. GST ($m$ ~ 102) is more fragile than SST (m ~ 64) at temperatures approaching T_g. But importantly, a single fragility model can only work well in representing the viscosity behavior of SST for the high-temperature regime at above ~440 K, generating a rather large fragility m' > 170. Instead, the generalized-MYEGA model is able to simultaneously fit well both the low-temperature Arrhenius (ranging from 10 to 2000 K s^{-1}) and high-temperature super-Arrhenius terms in the Kissinger plot (Figure S1 in the Supporting Information), while the MYEGA model yields the breakdown of Arrhenius behavior as approaching the low temperature. These two fragility scenarios strongly indicate that there is a considerable change in fragility, resulting in large contrast in kinetics, at around 440 K, which can be attributed to an apparent fragile-to-strong (FTS) crossover in the deeply supercooled SST liquid (Figure 3b): the Arrhenius behavior is approximately obeyed from T_g to $T_g/T \approx 0.85$ (i.e., ~371−436 K); but a super-Arrhenius behavior emerges as the temperature further increases, with η sharply dropping toward that of GST beyond $T_g/T \approx 0.65$ (i.e., T > ~570 K). The FTS crossover can be assessed by monitoring $E_\eta = k_B d\ln(\eta/\eta_0)/d(1/T)$, where k_B is the Boltzmann constant and E_η is the activation energy of viscosity. The E_η of SST increases upon cooling until a clear plateau appears (inset of Figure 3b), and an inflection point is seen at ~445 K, which can be taken as the FTS temperature for SST. In contrast, no clear FTS crossover can be observed in GST above T_g.[15,25]

The FTS crossover was also observed in many other chalcogenide films, such as $Ge_{15}Te_{85}$[34,35] and AIST,[25,36,37] as well as GST[26] and GeTe[38] nanoparticles, which may originate from the increase of Peierls distortion[39] in short range, and the formation of an energetically favorable network at or beyond medium range, during quenching of the supercooled liquid.[40,41] As Peierls distortion increases, electrons become more localized between atoms, exerting constraints on atomic migration and consequently increasing the activation barrier of viscous flow. An enhanced kinetic contrast due to FTS crossover thus enables high atomic mobility at elevated temperatures for rapid crystal growth and suffocated atomic diffusion near room temperature for good data retention. In contrast to the FTS crossover in good-glass formers (e.g., $Ge_{15}Te_{85}$), which occurs near or even above T_m, causing very viscous flow and sluggish crystallization,[34,35] to be conducive to superior cache-type nonvolatile PCMs, it is desirable for the FTS crossover to happen right below the typical programming temperatures for crystallization, e.g., <~600−700 K, and considerably above T_g, e.g., >~400 K. This is the case for SST, as shown above. It is also worth noting that the nanosized confinement of PCMs can further enlarge the kinetic contrast,[42,43] which may come in handy when high-density cache-type nonvolatile PCRAM is developed through device geometry miniaturization.

Heterogeneous Versus Homogeneous Nucleation. The viscosity in the temperature regime above T_g strongly influences the nucleation dynamics. A larger viscosity, accompanied by a higher temperature for the crossover to

DOI: 10.1021/acs.chemmater.9b02598
Chem. Mater. 2019, 31, 8794−8800

fragile liquid, suppresses nucleation in the supercooled liquids.[24,25,37] The steady-state nucleation rate (I^{ss}) in SST below ~700 K, estimated in the Supporting Information using classical nucleation theory[44] for homogeneous nucleation, is about 7−16 orders of magnitude lower than that of GST (Figure 4a). Note that $\xi = 1$ is applied to both GST and SST for calculating the I^{ss} and the effective time lag τ^* of homogeneous nucleation, as Stokes−Einstein relation is well complied with during nucleation.[24] The I^{ss} for both GST and SST reaches a maximum at ~520 K. At temperatures below ~500 K, the time lag of homogeneous nucleation (τ^*, see the Supporting Information), i.e., the incubation time for critical-sized nuclei,[2,24] is ~1−2 orders of magnitude longer in SST than in GST (Figure 4b).

All of the above features, namely, lower U, smaller I^{ss}, and longer τ^* for homogeneous nucleation act against the much faster crystallization of SST over GST. Clearly, the superior SET speed of SST must be due to heterogeneous nucleation, where Sc−Te-based precursors act as preformed heterogeneous nucleation sites.[12] This can be envisioned as follows. With Sc additions, the high-fidelity precursors due to Sc−Te cubes can play an effective role in reducing the interfacial energy to catalyze crystal nuclei.[12] The heterogeneous I^{ss} of SST, assuming a contact angle θ of 60°, is ~7−15 orders of magnitude higher than the homogeneous I^{ss} of GST at ~600−700 K (Figure 4a, see the Supporting Information for calculations). At the crystallization temperature of ~600−700 K, in GST, the stochastic homogeneous I^{ss} drops by ~8 orders of magnitude from the peak value at ~520 K. In contrast, in SST, the heterogeneous I^{ss} remains steadily high until ~700 K, dropping less than ~3 orders from the maximum. Note that in this analysis, the contact angle is only an assumption; however, upon adjusting its value, we found that as long as it is below 90°, the maximum heterogeneous I^{ss} of SST surpasses the homogeneous I^{ss} of GST by a large margin (Figure 4a). The comparison here already suffices to prove our point: it is an adequate number of robust Sc−Te precursors/motifs serving as heterogeneous sites that substantially reduce the stochasticity in nucleation to enable the rapid SET operation of SST. Note, however, that one cannot arbitrarily increase Sc doping to very high levels; that may have a negative impact,[45] because an excessive population of Sc-stabilized motifs would then reduce atomic diffusion considerably, which would slow down the nucleation and growth in crystallization.

CONCLUSIONS

We performed ultrafast DSC experiments on SST, which is a promising PCM for realizing cache-type nonvolatile PCRAM, owing to its subnanosecond crystallization speed in SET operation and long-term data reliability of the RESET amorphous state. These two "conflicting" properties of SST can be reconciled, from the temperature dependence of the crystallization dynamics in the supercooled liquid regime. From experimental ultrafast DSC data, we have derived that (i) below ~570 K, supercooled liquid SST has a higher viscosity than GST, resulting in ~1−2 orders of magnitude slower crystal growth velocity. (ii) At its peak near T = 630 K, the maximum growth velocities of both PCMs are comparable, ~2 m·s^{-1}, but SST has a slightly faster growth velocity at higher temperatures. (iii) SST exhibits a broader range of Arrhenius dynamics with higher activation energy than GST. (iv) SST shows a stronger contrast in kinetics, with an FTS crossover at ~445 K, while GST does not have such a transition. All these explain the good attribute of reliable data retention of SST: it is highly resistant to crystallization due to diminishing kinetics at low temperatures. Meanwhile, SST delivers faster SET operation than GST at elevated temperatures. This is because, although SST supercooled liquid does not favor homogeneous nucleation more than GST, the former relies on heterogeneous sites on Sc−Te-based precursors to drastically accelerate the crystal nucleation, when the temperature is sufficiently elevated to above the crossover to fragile liquid, where kinetics are no longer a problem. Taken all of the above together, our work illustrates a route to superior PCMs conducive to cache-type nonvolatile PCRAM devices. The take-home message is that to avoid a trade-off between fast crystallization speed and sustainable amorphous state for data retention, the way to go is to promote crystal nucleation rate at elevated temperatures, while enlarging the kinetic contrast for crystal growth between high and low temperatures. In this regard, SST serves as a good example to demonstrate this desirable behavior in terms of nucleation and growth kinetics.

METHODS

Film Preparation. The ~300 nm-thick SST films were deposited on a SiO_2/Si substrate at room temperature by co-sputtering pure Sc and Sb_2Te_3 targets in ultrahigh vacuum with a base pressure of <~2 × 10^{-7} mTorr. The deposition rate was controlled to be ~5 nm min^{-1}. SiO_2 capping layer (~10 nm thick) was in situ grown on top of the SST film inside the vacuum chamber to avoid oxidation. The compositions of SST films were measured using X-ray fluorescence spectroscopy (Rigaku RIX 2100).

Ultrafast DSC. Power-compensation DSC was performed using a Mettler-Toledo Flash DSC 1 instrument with the sensor chips (USF-1), each containing working and reference area. The SST small flakes were scraped off from the substrate and then transferred onto the working area of the chip sensor. The heating rates Φ varied from 10 to 40 000 K·s^{-1}. At each Φ, measurements were repeated at least three times for low Φ and 5−10 times for high Φ, as the values of the crystallization temperature become more scattered at high Φ. Thermal lag and temperature calibration of the Ultrafast DSC are evaluated in detail in the Supporting Information. A detailed methodology of the Kissinger fitting can be seen in our previous work.[38] The viscosity model used in this work is illustrated in the Supporting Information. Since the SST flakes were only one-side capped, it is appropriate to compare the ultrafast DSC results with those of uncapped GST films[15] and not with the sandwiched GST films.[43]

Device Fabrication and Electrical Characterization. T-shaped PCRAM devices with tungsten bottom electrode contact of ~190 nm in diameter were fabricated using the 0.13 μm node complementary metal-oxide-semiconductor technology.[12] The thickness of the PCM films of all of the devices was controlled to be ~150 nm. The ~15 nm-thick TiN and ~300 nm-thick Al films were used as top electrode in all devices. The electrical measurements were performed by using the Keithley 2400C source meter (measuring device resistance), the Tektronix AWG5002B pulse generator (generating nanoseconds voltage pulse with a minimum width of ~6 ns), and the Picosecond Pulse Labs Model 10070A pulse generator (generating picoseconds voltage pulse with a minimum width of ~100 ps and a maximum magnitude of ~7.5 V).

ASSOCIATED CONTENT

Supporting Information

The Supporting Information is available free of charge on the ACS Publications website at DOI: 10.1021/acs.chemmater.9b02598.

Viscosity model description; thermal lag evaluation in ultrafast differential scanning calorimetry; classical

DOI: 10.1021/acs.chemmater.9b02598
Chem. Mater. 2019, 31, 8794−8800

nucleation theory to model the steady-state nucleation rate of $Sc_{0.2}Sb_2Te_3$ phase-change material (PDF)

AUTHOR INFORMATION

Corresponding Author

*E-mail: fengrao@szu.edu.cn.

ORCID

Bin Chen: 0000-0003-1591-0843
Yimin Chen: 0000-0002-3057-5062
Lei Wang: 0000-0002-2313-2095
Wei Zhang: 0000-0002-0720-4781
Feng Rao: 0000-0002-6922-5393

Author Contributions

B.C., Y.C., and K.D. contributed equally to this work. K.L., F.J., and K.D. fabricated the SST films for ultrafast DSC tests. Y.C., J.W., and X.S. performed ultrafast DSC measurements. B.C. and Y.C. performed simulation and fitting. K.D. and F.R. prepared the device samples and carried out electrical measurements. B.C., F.R., and E.M. wrote the paper with contributions from W.Z., L.W., and X.Z. All authors discussed the results and commented on the manuscript.

Notes

The authors declare no competing financial interest.

ACKNOWLEDGMENTS

F.R. gratefully thanks the support of National Natural Science Foundation of China (61622408), the Major Provincial Basic Research Program of Guangdong (2017KZDXM070), and the Science and Technology Foundation of Shenzhen (JCYJ20180507182248605). Y.C. thanks the support of National Natural Science Foundation of China (61904091). J.W. thanks the support of National Natural Science Foundation of China (51771216). X.S. thanks the support of National Natural Science Foundation of China (61775111). W.Z. thanks the support of National Natural Science Foundation of China (61774123). E.M. is supported at Johns Hopkins University by U.S. DOE-BES-DMSE under grant DE-FG02-19ER46056.

REFERENCES

(1) Wuttig, M.; Yamada, N. Phase-Change Materials for Rewriteable Data Storage. *Nat. Mater.* **2007**, *6*, 824−832.

(2) Raoux, S.; Welnic, W.; Ielmini, D. Phase Change Materials and Their Application to Nonvolatile Memories. *Chem. Rev.* **2010**, *110*, 240−267.

(3) Kolobov, A. V.; Fons, P.; Frenkel, A. I.; Ankudinov, A. L.; Tominaga, J.; Uruga, T. Understanding the Phase-Change Mechanism of Rewritable Optical Media. *Nat. Mater.* **2004**, *3*, 703−708.

(4) Lencer, D.; Salinga, M.; Wuttig, M. Design Rules for Phase-Change Materials in Data Storage Applications. *Adv. Mater.* **2011**, *23*, 2030−2058.

(5) Li, X.-B.; Chen, N.-K.; Wang, X.-P.; Sun, H.-B. Phase-Change Superlattice Materials toward Low Power Consumption and High Density Data Storage: Microscopic Picture, Working Principles, and Optimization. *Adv. Funct. Mater.* **2018**, *28*, No. 1803380.

(6) Wuttig, M. Phase-Change Materials: Towards a Universal Memory? *Nat. Mater.* **2005**, *4*, 265−266.

(7) Wong, H.-S. P.; Salahuddin, S. Memory Leads the Way to Better Computing. *Nat. Nanotechnol.* **2015**, *10*, 191−194.

(8) Atwood, G. Phase-Change Materials for Electronic Memories. *Science* **2008**, *321*, 210−211.

(9) Hegedüs, J.; Elliott, S. R. Microscopic Origin of the Fast Crystallization Ability of Ge−Sb−Te Phase-Change Memory Materials. *Nat. Mater.* **2008**, *7*, 399−405.

(10) Ielmini, D.; Lacaita, A. L. Phase Change Materials in Non-Volatile Storage. *Mater. Today* **2011**, *14*, 600−607.

(11) Choe, J. Tech Insights: Intel 3D XPoint Memory Die Removed from Intel Optane PCM (Phase Change Memory), https://www.techinsights.com/blog/intel-3d-xpoint-memory-die-removed-intel-optanetm-pcm-phase-change-memory (accessed May 18, 2017).

(12) Rao, F.; Ding, K.; Zhou, Y.; Zheng, Y.; Xia, M.; Lv, S.; Song, Z.; Feng, S.; Ronneberger, I.; Mazzarello, R.; et al. Reducing the Stochasticity of Crystal Nucleation to Enable Subnanosecond Memory Writing. *Science* **2017**, *358*, 1423−1427.

(13) Zhang, W.; Mazzarello, R.; Wuttig, M.; Ma, E. Designing Crystallization in Phase-Change Materials for Universal Memory and Neuro-Inspired Computing. *Nat. Rev. Mater.* **2019**, *4*, 150−168.

(14) Rao, F.; Song, Z.; Cheng, Y.; Liu, X.; Xia, M.; Li, W.; Ding, K.; Feng, X.; Zhu, M.; Feng, S. Direct Observation of Titanium-Centered Octahedra in Titanium−Antimony−Tellurium Phase-Change Material. *Nat. Commun.* **2015**, *6*, No. 10040.

(15) Orava, J.; Greer, A. L.; Gholipour, B.; Hewak, D. W.; Smith, C. E. Characterization of Supercooled Liquid $Ge_2Sb_2Te_5$ and Its Crystallization by Ultrafast-Heating Calorimetry. *Nat. Mater.* **2012**, *11*, 279−283.

(16) Kalikka, J.; Akola, J.; Jones, R. O. Simulation of Crystallization in $Ge_2Sb_2Te_5$: A Memory Effect in the Canonical Phase-Change Material. *Phys. Rev. B* **2014**, *90*, No. 184109.

(17) Kalikka, J.; Akola, J.; Jones, R. O. Crystallization Processes in the Phase Change Material $Ge_2Sb_2Te_5$: Unbiased Density Functional/Molecular Dynamics Simulations. *Phys. Rev. B* **2016**, *94*, No. 134105.

(18) Akola, J.; Jones, R. O. Structural Phase Transitions on the Nanoscale: The Crucial Pattern in the Phase-Change Materials $Ge_2Sb_2Te_5$ and GeTe. *Phys. Rev. B* **2007**, *76*, No. 235201.

(19) Ronneberger, I.; Zhang, W.; Eshet, H.; Mazzarello, R. Crystallization Properties of the $Ge_2Sb_2Te_5$ Phase-Change Compound from Advanced Simulations. *Adv. Funct. Mater.* **2015**, *25*, 6407−6413.

(20) Cheng, H. Y.; Hsu, T. H.; Raoux, S.; Wu, J. Y.; Du, P. Y.; Breitwisch, M.; Zhu, Y.; Lai, E. K.; Joseph, E.; Mittal, S. et al. In *A High Performance Phase Change Memory with Fast Switching Speed and High Temperature Retention by Engineering the Ge_xSb_yTezphase Change Material*. 2011 International Electron Devices Meeting, 2011; pp 3.4.1−3.4.4.

(21) Lee, T. H.; Loke, D.; Elliott, S. R. Microscopic Mechanism of Doping-Induced Kinetically Constrained Crystallization in Phase-Change Materials. *Adv. Mater.* **2015**, *27*, 5477−5483.

(22) Yamada, N.; Ohno, E.; Nishiuchi, K.; Akahira, N.; Takao, M. Rapid-phase Transitions of GeTe-Sb_2Te_3 Pseudobinary Amorphous Thin Films for an Optical Disk Memory. *J. Appl. Phys.* **1991**, *69*, 2849−2856.

(23) Loke, D.; Lee, T. H.; Wang, W. J.; Shi, L. P.; Zhao, R.; Yeo, Y. C.; Chong, T. C.; Elliott, S. R. Breaking the Speed Limits of Phase-Change Memory. *Science* **2012**, *336*, 1566−1569.

(24) Orava, J.; Greer, A. L. Classical-Nucleation-Theory Analysis of Priming in Chalcogenide Phase-Change Memory. *Acta Mater.* **2017**, *139*, 226−235.

(25) Orava, J.; Hewak, D. W.; Greer, A. L. Fragile-to-Strong Crossover in Supercooled Liquid Ag-In-Sb-Te Studied by Ultrafast Calorimetry. *Adv. Funct. Mater.* **2015**, *25*, 4851−4858.

(26) Chen, B.; ten Brink, G. H.; Palasantzas, G.; Kooi, B. J. Crystallization Kinetics of GeSbTe Phase-Change Nanoparticles Resolved by Ultrafast Calorimetry. *J. Phys. Chem. C* **2017**, *121*, 8569−8578.

(27) Chen, Y.; Wang, G.; Song, L.; Shen, X.; Wang, J.; Huo, J.; Wang, R.; Xu, T.; Dai, S.; Nie, Q. Unraveling the Crystallization Kinetics of Supercooled Liquid GeTe by Ultrafast Calorimetry. *Cryst. Growth Des.* **2017**, *17*, 3687−3693.

DOI: 10.1021/acs.chemmater.9b02598
Chem. Mater. 2019, 31, 8794−8800

(28) Russo, U.; Ielmini, D.; Lacaita, A. L. Analytical Modeling of Chalcogenide Crystallization for PCM Data-Retention Extrapolation. *IEEE Trans. Electron Devices* **2007**, *54*, 2769−2777.
(29) Wuttig, M.; Salinga, M. Phase-Change Materials: Fast Transformers. *Nat. Mater.* **2012**, *11*, 270−271.
(30) Sebastian, A.; Le Gallo, M.; Krebs, D. Crystal Growth within a Phase Change Memory Cell. *Nat. Commun.* **2014**, *5*, No. 4314.
(31) Jeyasingh, R.; Fong, S. W.; Lee, J.; Li, Z.; Chang, K.-W.; Mantegazza, D.; Asheghi, M.; Goodson, K. E.; Wong, H.-S. P. Ultrafast Characterization of Phase-Change Material Crystallization Properties in the Melt-Quenched Amorphous Phase. *Nano Lett.* **2014**, *14*, 3419−3426.
(32) Park, J.; Kim, M. R.; Choi, W. S.; Seo, H.; Yeon, C. Characterization of Amorphous Phases of $Ge_2Sb_2Te_5$ Phase-Change Optical Recording Material on Their Crystallization Behavior. *Jpn. J. Appl. Phys.* **1999**, *38*, No. 4775.
(33) Angell, C. A. Formation of Glasses from Liquids and Biopolymers. *Science* **1995**, *267*, 1924−1935.
(34) Weber, H.; Orava, J.; Kaban, I.; Pries, J.; Greer, A. L. Correlating Ultrafast Calorimetry, Viscosity, and Structural Measurements in Liquid GeTe and $Ge_2Sb_2Te_5$. *Phys. Rev. Mater.* **2018**, *2*, No. 093405.
(35) Wei, S.; Stolpe, M.; Gross, O.; Hembree, W.; Hechler, S.; Bednarcik, J.; Busch, R.; Lucas, P. Structural Evolution on Medium-Range-Order during the Fragile-Strong Transition in $Ge_{15}Te_{85}$. *Acta Mater.* **2017**, *129*, 259−267.
(36) Salinga, M.; Carria, E.; Kaldenbach, A.; Bornhöfft, M.; Benke, J.; Mayer, J.; Wuttig, M. Measurement of Crystal Growth Velocity in a Melt-Quenched Phase-Change Material. *Nat. Commun.* **2013**, *4*, No. 2371.
(37) Zalden, P.; von Hoegen, A.; Landreman, P.; Wuttig, M.; Lindenberg, A. M. How Supercooled Liquid Phase-Change Materials Crystallize: Snapshots after Femtosecond Optical Excitation. *Chem. Mater.* **2015**, *27*, 5641−5646.
(38) Chen, B.; de Wal, D.; ten Brink, G. H.; Palasantzas, G.; Kooi, B. J. Resolving Crystallization Kinetics of GeTe Phase-Change Nanoparticles by Ultrafast Calorimetry. *Cryst. Growth Des.* **2018**, *18*, 1041−1046.
(39) Chen, N.-K.; Li, X.-B.; Bang, J.; Wang, X.-P.; Han, D.; West, D.; Zhang, S.; Sun, H.-B. Directional Forces by Momentumless Excitation and Order-to-Order Transition in Peierls-Distorted Solids: The Case of GeTe. *Phys. Rev. Lett.* **2018**, *120*, No. 185701.
(40) Zalden, P.; Quirin, F.; Schumacher, M.; Siegel, J.; Wei, S.; Koc, A.; Nicoul, M.; Trigo, M.; Andreasson, P.; Enquist, H.; et al. Femtosecond X-Ray Diffraction Reveals a Liquid−Liquid Phase Transition in Phase-Change Materials. *Science* **2019**, *364*, 1062−1067.
(41) Rao, F.; Zhang, W.; Ma, E. Catching Structural Transitions in Liquids. *Science* **2019**, *364*, 1032−1033.
(42) Salinga, M.; Kersting, B.; Ronneberger, I.; Jonnalagadda, V. P.; Vu, X. T.; Gallo, M. L.; Giannopoulos, I.; Cojocaru-Mirédin, O.; Mazzarello, R.; Sebastian, A. Monatomic Phase Change Memory. *Nat. Mater.* **2018**, *17*, 681−685.
(43) Orava, J.; Greer, A. L.; Gholipour, B.; Hewak, D. W.; Smith, C. E. Ultra-Fast Calorimetry Study of $Ge_2Sb_2Te_5$ Crystallization between Dielectric Layers. *Appl. Phys. Lett.* **2012**, *101*, No. 091906.
(44) Kelton, K. F.; Greer, A. L.; Thompson, C. V. Transient Nucleation in Condensed Systems. *J. Chem. Phys.* **1983**, *79*, 6261−6276.
(45) Zewdie, G. M.; Zhou, Y.; Sun, L.; Rao, F.; Deringer, V. L.; Mazzarello, R.; Zhang, W. Chemical Design Principles for Cache-Type Sc−Sb−Te Phase-Change Memory Materials. *Chem. Mater.* **2019**, *31*, 4008−4015.

DOI: 10.1021/acs.chemmater.9b02598
Chem. Mater. 2019, 31, 8794−8800